Hydrogel Smart Bandage as a Diagnostic Tool for Infection in Burn Wounds

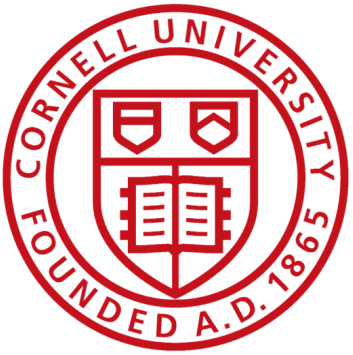

Keywords: hydrogel bandage, diffusion, fluorescence, COMSOL, infection

BEE 4530: Computer Aided Engineering | Applications to Biological Processes

May 2022

Table of Contents

1.1 Executive Summary:

Every year, almost half a million people are admitted to the emergency room because of burn wounds. Of the thousands of deaths that result from these wounds, more than half are due to complications from infection. An easy solution would be to administer antibiotics immediately, but this can lead to serious problems. When antibiotics are given, the majority of bacteria die, but a few with natural resistances may survive. These cells will eventually grow and reproduce, leading to the formation of bacterial cell lines that are resistant to current antibiotics. Currently, detection of infection requires evaluation by a medical professional to avoid taking antibiotics unnecessarily. Unfortunately, this method is very time consuming and may take several days to obtain test results such as blood or bacterial cultures. This option also may not be accessible in developing countries. Since infection can be fatal, it is beneficial to have a way to determine if a wound is infected without the need to visit a doctor and wait for test results. Here, we describe a smart hydrogel bandage that is able to detect when a burn wound has become infected.

We chose to model a hydrogel bandage designed by SmartWound PREDICT using COMSOL, a finite element analysis simulation software. This bandage consists of a thin block of agarose hydrogel. This block contains wells that hold lipid vesicles full of fluorescent dye. The dye is self-quenching, meaning that the dye will not fluoresce while it is present in large concentrations within the minute volume of the vesicle. Once the vesicles rupture, the concentration will decrease as the dye exits the vesicle, allowing the dye to fluoresce.

After a burn wound has occurred, the hydrogel bandage is placed over it. When the wound becomes colonized by bacteria (such that the immune system alone is insufficient in fending off the infection and medical intervention is required), the bacteria begin producing the pore-forming toxin alpha hemolysin (α-H). This toxin diffuses up through the bottom of the bandage and into the vesicle-containing wells. Upon contact with the α-H, the vesicles will lyse and release the dye, which will begin to fluoresce in the presence of UV light. The fluorescence will signify that the wound has become infected and that the wearer should seek medical treatment.

Our model investigates potential methods to minimize the time for fluorescent dye to be released after infection and maximize the time before the dye comes into contact with the skin. We want to be able to detect the presence of an infection quickly without allowing the dye to contaminate the wound. Because the safety data sheet recommends washing skin thoroughly with soap and water upon contact with the dye, we hope to minimize skin contact with the dye in our design.

We based our bandage design on the preexisting bandage designed by SmartWound. To validate our model, we compared our COMSOL model results to the results obtained with the SmartWound PREDICT bandage. We found that our bandage exhibited visible fluorescence after 4 hours, like theirs did. We also found a similar dye concentration in the bandage after a set period of time. The validation did require altering some of our model parameters to reflect the fact that we modeled a typical wound and they tested their bandage on a bacterial biofilm, but any changes that were made were numerical and did not alter the integrity of the model. To

investigate the effects of geometry, we also tested several slightly different bandage designs as well.

Based on the information gathered from our model, we can make several recommendations about potential improvements in bandage design. First, we recommend that the vesicle wells should have a lower concentration of vesicles. This would make the bandage less expensive to produce without changing how long it takes for the bandage to fluoresce after being placed in contact with an infected wound. Decreasing the agarose concentration of the hydrogel bandage would be another potential improvement because it also would contribute to decreasing the cost of the bandage. It is important to note, however, that decreasing the percentage of agarose would also affect the mechanical properties of the bandage. This is beyond the scope of our model, but it may be an important factor to consider. A third potential improvement to the bandage would be to change the type of dye contained in the vesicles. If the current dye (6-carboxyfluorescein) was replaced with a larger dye (like sulforhodamine B), it would take longer to reach the skin after being released from the vesicles. This alteration could contribute to lowering the risk that the wound will be contaminated with dye. Another significant benefit of sulforhodamine B is that it is stable at room temperature, unlike 6-carboxyfluorescein that must be refrigerated for long-term storage. This would allow the sulforhodamine B based bandage to be more accessible in developing countries. The drawback to this dye is that it is significantly more expensive than 6-carboxyfluorescein. This expense could be offset in part by the decrease in the concentration of vesicles in the well; if there are fewer vesicles there will be less dye to pay for.

Infection in burn wounds kills thousands of people every year. A bandage that informs its user when the wound is infected could drastically decrease the mortality rate, while also being a more convenient and accessible method for detecting infection.

2.1 Introduction:

Infections can be extremely dangerous. After a wound is formed, it can be only a matter of hours before bacteria colonize it [1]. The growth of bacteria in a wound follows an approximately exponential curve if left unchecked [2]. At a certain point during the infection, called the critical colonization threshold (CCT), the infectious bacteria will either continue to grow and require medical intervention, or the infection will be resolved naturally by the body's immune system [3]. If the bacteria continues to replicate, it will eventually reach the stationary phase, shown in Figure 1 as the portion of the graph where the red line levels off.

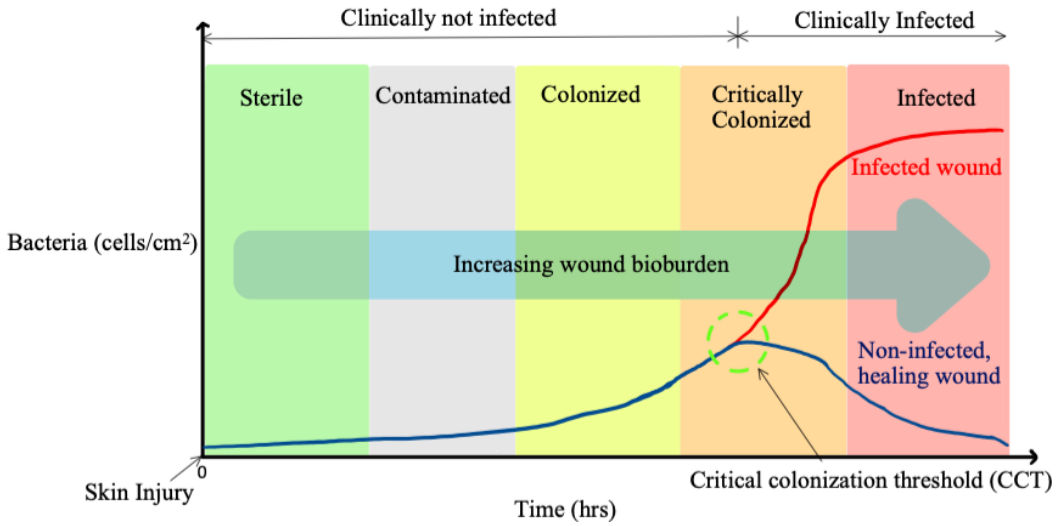

Figure 1: Timeline of bacterial colonization of a wound from. After the CCT, the red line shows the bacteria continuing to replicate and reaching the stationary phase, where the amount of bacteria in the wound is no longer changing.

Infections can be difficult to detect within burn wounds, often requiring medical examination and laboratory tests. Thus, it would be convenient to have a point-of-care diagnostic tool to detect and report the presence of an infection without a medical professional. One of the most common microbes involved in wound infections is *Staphylococcus aureus* [3]. It is also one of the most dangerous, as it is a predominant factor in delayed wound healing [4]. As such, we will approximate all bacteria in the wound as *S. aureus.* This microbe follows the same growth pattern as the general bacteria described in Figure 1. Like most bacteria, once the microbial load has reached stationary phase a wound is considered clinically infected and antibiotics should be used to prevent sepsis and scarring. At this same time, the colony reaches stationary phase and no longer replicates exponentially. Since not all of the energy has to go to replication, the bacteria can begin to use it for other things. Specifically, after reaching the stationary phase, *S. aureus* begins to use some of the energy that was once devoted to replication to produce high levels of many different pore-forming cytotoxins [5]. For our purposes, we will focus on alpha-hemolysin (α-H) as a representative cytotoxin in our model since all of the produced cytotoxins are structurally similar and thus share similar mechanisms of action as well as diffusivities. α-H forms pores in lipid bilayers, causing the cell membrane to lyse [7].

Without proper care, exponential growth of bacteria past the CCT can lead to sepsis or scarring. Antibiotics are a powerful tool for the treatment of bacterial infections, but their overuse can promote antibiotic resistance [6]. This could potentially have negative effects in the long term, as new strains become more and more resistant to treatment. Thus, it is important to know when it is appropriate to treat an infection with antibiotics and when the body's immune system will be able to take care of the infection without assistance. Today, most infection diagnostic tests require a visit to a doctor's office and blood tests or cultures. This method can be time consuming, inefficient, and is not universally accessible, allowing infections to progress

while waiting for an appointment or for results. To address this issue, we have chosen to model an agarose hydrogel bandage that will begin to glow if it is exposed to the cytotoxins produced by an infected burn wound.

Our hydrogel bandage will contain wells filled with lipid vesicles holding the fluorescent dye 6-carboxyfluorescein. While in the vesicles, the fluorescence from the dye will not be visible because the dye molecules are self-quenching (which means at extremely high concentrations, the dye molecules dimerize and no longer fluoresce) [8]. When the vesicles come into contact with α-H after it diffuses up from the wound, the α-H will form pores in the vesicles and release the fluorescent dye. Once released, the fluorescent dye dimers will diffuse out from the vesicles into the bandage, and at these lower concentrations the dye will undimerize and fluoresce. As such, the user will be able to see this dye under UV light and know that the wound is severely infected and requires medical intervention.

2.2 Problem Statement:

We will use COMSOL to model this SmartWound PREDICT bandage. Using this model, we will investigate how α-H produced from *S. aureus* in an open, circular burn wound will diffuse through a hydrogel bandage and react with dye-filled lipid vesicles. Thus, the bandage fluorescing should indicate an infection that requires medical intervention. We will also model how fluorescent dye is released from the lysed vesicles in the wells of our hydrogel and examine how it diffuses into the hydrogel bandage. Our geometry is in 3D (Figure 2) and our domain includes the hydrogel bandage and the wound. In order to measure the success of our model, we will also model the concentration of fluorescent dye released from the vesicles over time.

2.3 Design Objectives:

We will design a hydrogel dressing that will glow when placed over an infected wound. To do this we will need to:

- Develop mass transfer models for α-H and fluorescent dye throughout the hydrogel smart bandage and the circular burn wound. Model will require a 3D geometry due to the presence of asymmetry across the x,y-plane.
- Understand how hydrogel composition and fluorescent dye type influence how quickly α-H can diffuse into the hydrogel wells and release the fluorescent dye to signal the user that medical intervention is needed.
- Understand how hydrogel composition, hydrogel bandage dimensions, and fluorescent dye type influence how quickly fluorescent dye can diffuse through the hydrogel bandage and reach the wound.
- Redesign the hydrogel smart bandage to minimize the time it takes for α-H to diffuse into the wells and release the fluorescent dye while maximizing the time it takes fluorescent dye to diffuse into the wound and contaminate it.

3. Methods

3.1 Schematic:

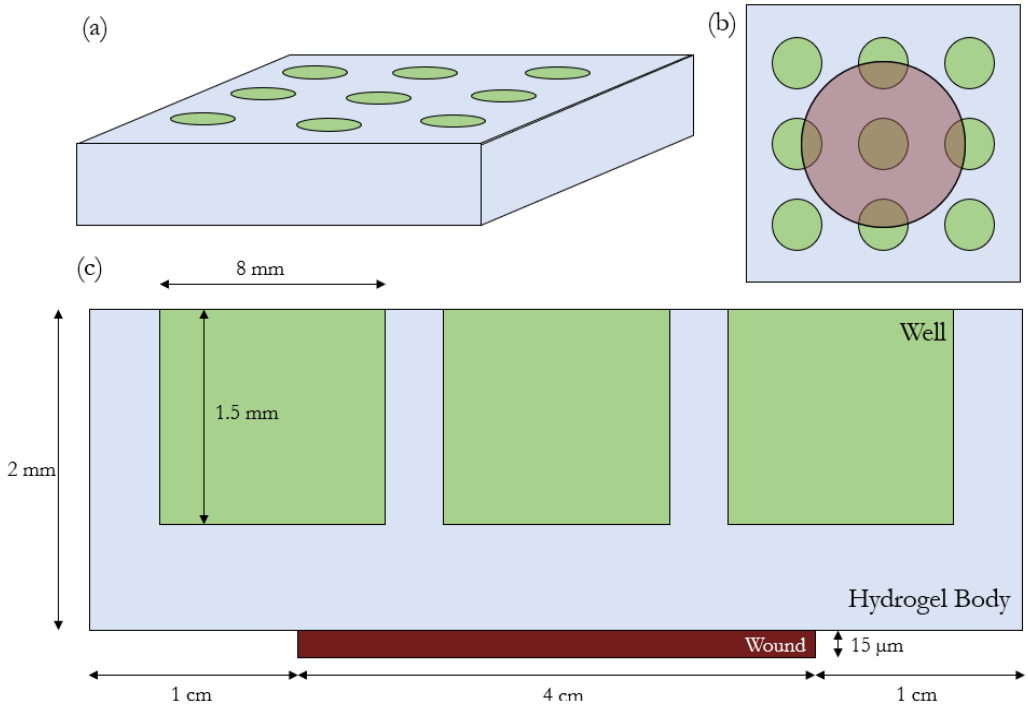

Figure 2: Schematic of the domain to be modeled. (a) Three dimensional structure of the bandage. (b) Top view of the bandage, with the wound superimposed in brown. (c) Cross section of the bandage cut through its center. The dimensions implemented in COMSOL are as shown. The cylindrical wells containing vesicles are shown in green.

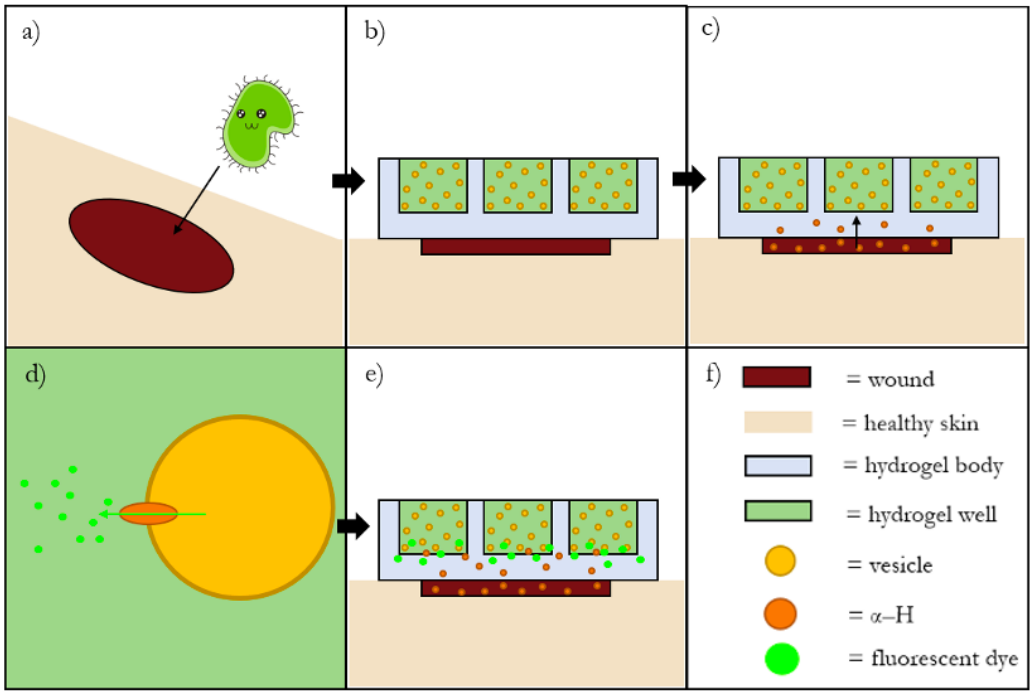

Figure 3: Infection detection process. First, a wound occurs and is colonized by bacteria (a). The Smart Bandage is then placed over the wound (b). Once the bacteria reach stationary phase, they spend more resources on generating

α-H, drastically increasing α-H concentration in the wound. The α-H then diffuses up through the bandage (c). When the α-H reaches the vesicles in the hydrogel wells, the vesicles react with seven α-H to create a pore that releases fluorescent dye. In our model, this is a pseudo reaction that requires one vesicle and 7 α-H to create 80 molecules of fluorescent dye (d). Finally, the dye diffuses throughout the bandage, indicating that the wound is infected (e).

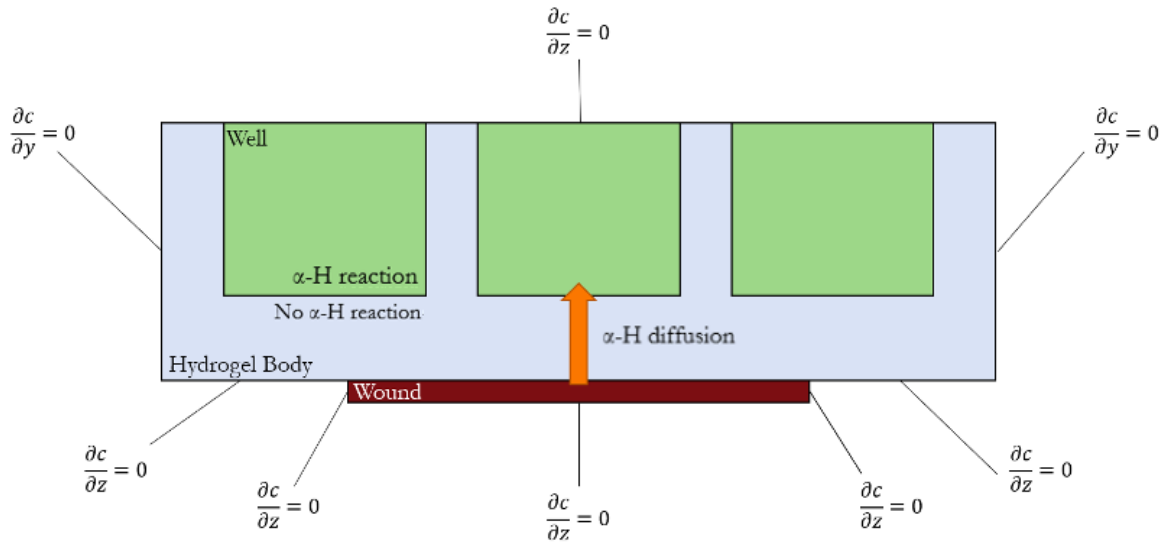

Figure 4: Boundary conditions for diffusion of α-H and dye. As shown in the diagram, zero-flux boundary conditions can be used all around the bandage, as neither α-H nor dye will be able to leave the bandage through convection. Zero-flux boundary conditions can be used in the wound due to its shallow nature and the cauterizing effect of burns. The α-H reacts only in the wells and not in the hydrogel body. The green wells have the same diffusivity as the hydrogel body; the green is added to show the reaction domains.

3.2 General Assumptions:

In order to translate the processes in this smart bandage into a COMSOL model, several assumptions need to be made. As stated in the introduction, we will assume that all of the bacteria in the wound are *S. aureus* for simplicity purposes since *S. aureus* is one of the most common microbes that infect wounds [3]. We will also assume that the *S. aureus* distributes evenly throughout the wound, and concentrates at the wound surface due to exposure to oxygen [2]. We can assume a constant concentration of lipid vesicles in the wells due to the following logic: human plasma has a concentration of $2 \cdot 10^{10}$ vesicles/mL, which would be significantly lower than the concentration of vesicles within our wells [9]. Using this concentration and the fact that the wound only releases approximately 5000 α-H pores per second and assuming that somehow, all these pores make it into the 1 mL containing these vesicles, it would take several weeks to use up all the vesicles. Considering that our ideal time-scale for this device would be within several hours, it's safe to assume that the vesicle concentration would not change in any appreciable amount. Another assumption we can make is that only 1 α-H pore will form per vesicle. We can assume this because the vesicles are about 0.5 μm^2 in surface area and the maximum distribution for α-H pores in a lipid bilayer was calculated to be ~4 μm^2 in between each pore [10]. Given this distribution, it is only possible for one to form in each vesicle.

3.3 Governing Equations:

The governing equation describing this problem is the transient mass transfer equation:

$$\frac{\partial c}{\partial t} + \left(u_x \frac{\partial c}{\partial x} + u_y \frac{\partial c}{\partial y} + u_z \frac{\partial c}{\partial c_z}\right) = D_A\left(\frac{\partial^2 c}{\partial x^2} + \frac{\partial^2 c}{\partial y^2} + \frac{\partial^2 c}{\partial z^2}\right) + R \quad (1)$$

Convection (the second term from the left) is ignored because the skin tissue around the burn wound is naturally cauterized by the heat that initially formed the burn, preventing blood from reaching and flowing through the wound [11]. We included the diffusive mass transfer term since it is the dominant means of mass transfer in this process. To model this device, we decided to model the mass transfer of two species (fluorescent dye and α-H) through three main domains (Figure 4): the wound, the hydrogel main body, and the hydrogel well. The final governing equation for the system is:

$$\frac{\partial c}{\partial t} = D\ \left(\frac{\partial^2 c}{\partial x^2} + \frac{\partial^2 c}{\partial y^2} + \frac{\partial^2 c}{\partial z^2}\right) + R \quad (2)$$

Within different domains and for different species, there are different values for each term in the transient mass transfer equation (Figure 5).

$$R = \begin{Bmatrix} R_{\alpha-H,volumetric} & \alpha - \text{H in wound} \\ R_{\alpha-H,volumetric} & \alpha - \text{H in well} \\ R_{dye,volumetric} & \text{dye in well} \\ 0 & \text{otherwise} \end{Bmatrix}$$

$$D = \begin{Bmatrix} D_{\alpha-H,wound} & \alpha - \text{H in wound} \\ D_{\alpha-H,gel} & \alpha - \text{H in hydrogel} \\ D_{dye,wound} & \text{dye in well} \\ D_{dye,gel} & \text{dye in hydrogel} \end{Bmatrix}$$

$$c = \begin{Bmatrix} c_{dye} & \text{concentration of dye} \\ c_{\alpha-H} & \text{concentratioin of } \alpha - \text{H} \end{Bmatrix}$$

Figure 5: Variable names to substitute into the governing equation (Equation 2) based on domain and species. Variable values are in the appendix. The reaction term for α-H in the wells is referring to the reaction with the vesicles that consumes α-H monomers.

3.4 Determination of Parameters in the Governing Equations:

The values for the diffusivities of α-H and dye in the domains were found through literature searches. These values and their sources are cataloged in the appendix. The determination of the reaction term for each species of interest in each domain was more involved. There were three non-zero reaction terms to take into account: production of α-H in the wound, removal of α-H in the well, and production of fluorescent dye in the well.

3.4.1 α-H Production in Wound:

The determination of the rate of α-H production in the wound relied on several of our assumptions. First, we made the assumption that we are modeling the moment the bacteria in the wound reach stationary phase and onward. Since the bacteria are at stationary phase, the population is stable and we can use a constant number of bacteria. Second, we rely on the assumption that the bacteria are evenly distributed in the top 15 μm of the wound for easy access

to oxygen [2]. This allows us to model the bacteria concentration as constant throughout the wound. Together, these assumptions allow us to use a single constant as the production rate of α-H in the wound.

To find this production rate, we used the following information. At stationary phase, the concentration of bacteria in the wound is 110,900 bacteria per cm^3 of tissue and each bacterium produces 6.4 μg of α-H per second per mg of dry weight [4]. Since each bacteria has an average dry weight of $1.5 \cdot 10^{-10}$mg, this equates to $9.6 \cdot 10^{-10}$ng of α-H monomers per second per bacteria. Given the weight of an α-H monomer and the concentration of bacteria in the wound, we find the net production of α-H monomers in the wound to be 2×10^6 monomers per cubic centimeter per second with the following calculation.

$$R_{\alpha-H,\,volumetric} = 9.6 \cdot 10^{-10} \frac{ng\ \alpha-H}{bacteria \cdot s} \cdot 110900\ \frac{bacteria}{cm^3} \cdot \frac{1}{5.4 \cdot 10^{-11}} \frac{molecules\ \alpha-H}{ng\ \alpha-H} = 2 \cdot 10^6 \frac{molecules\ \alpha-H}{cm^3 \cdot s} \quad (3)$$

3.4.2 α-H Degradation in Wells:

The rate of α-H irreversibly binding to the vesicles in the wells was modeled as degradation. This rate of degradation was derived using Equation 4 [12].

$$\frac{dR_B}{dt} = k_{on} c_{A,\,weight} \left(1 - \frac{R_B}{R_{B,max}}\right) \quad (4)$$

In this equation, R_B is the mass of α-H adsorbed per unit area (ng/cm^2), $c_{A,weight}$ is the concentration of α-H in the wells (ng/cm^3), and k_{on} is the adsorption constant. Since $R_{B,\,max}$ is much greater than R_B due to the high vesicle concentration in the wells, the ratio of $R_B/R_{B,max}$ can go to 0, leaving us with a first order reaction. We are not, however, interested in the rate of α-H mass absorption per square centimeter of vesicle surface area. Instead, we want the rate of α-H absorption in moles per cubic centimeter of well. To transform this into the appropriate form, we can multiply both sides by the inverse of the weight of a single monomer of α-H and Avogadro's number. This puts concentration into the appropriate units (moles per cubic centimeter). Then, we can multiply by the surface area of a vesicle and the concentration of vesicles in the well. This puts k into the correct units (1/s). We will refer to this new value of k as k_{eff}. These conversions yield Equation 5 describing the rate of α-H monomers being adsorbed per cubic centimeter of well volume.

$$R_{\alpha-H,\,well} = -k_{eff} c_{\alpha-H} \quad (5)$$

In this equation, the negative sign denotes the fact that the α-H is being used up instead of produced.

3.4.3 Dye Production in Wells:

Seven α-H monomers combine in each vesicle to form a single pore. This pore allows the release of all of the dye contained within the vesicle. Since one pore can form in each vesicle, we can simply model the release of dye as a scaled consumption of α-H. Since each vesicle contains 80 molecules of dye and is lysed by a single pore, scaling Equation 4 by 80/7 gives us the production rate of fluorescent dye in the wells. This equation is positive since the dye is being released into the bandage.

$$R_{dye,well} = \frac{80}{7} k_{eff} c_{\alpha-H} \quad (6)$$

All of the other reaction rates will be zero. This is because in the wound and hydrogel main body, the dye is unaffected. Similarly, in the hydrogel main body the α-H is unaffected.

3.5 Boundary Conditions:

3.5.1 Wound:

Since we are modeling this bandage for use with burn victims, there will be zero flux boundary conditions for both α-H and dye at the borders of the wound. This is because burns essentially cauterize surrounding flesh, sealing off blood vessels and making the skin impermeable [11]. Since the skin is impermeable, the α-H and dye will not be able to diffuse through, and we can use a zero-flux boundary condition for both.

3.5.2 Hydrogel Main Body:

The edges of the hydrogel main body have zero-flux boundary conditions. This is because neither the dye nor the α-H can evaporate out of the gel. Against the skin the same boundary conditions apply, thanks to the cauterizing effect of burn wounds [11]. This is supported by the fact that the cytotoxin we are examining (α-H) only interacts with endothelial tissue not dermal or epidermal tissue [13].

3.5.3 Hydrogel Wells:

In this situation, the boundary conditions at the top of the hydrogel wells are continuous with the upper face of the hydrogel main body. Since neither the α-H nor the dye can diffuse out of the well, this entire face of the bandage can be modeled using a single zero-flux boundary condition.

3.6 Initial Conditions:

As shown in Figure 1, when a wound becomes critically infected the bacteria reach stationary phase. In stationary phase, the concentration of bacteria in the wound is at a constant level (in essence, the bacteria have reached the carrying capacity of the wound environment, and the rate of bacterial growth is equal to the rate of bacterial death). Since the bacteria no longer need to devote all of their resources to growing and colonizing the wound, they begin to produce cytotoxins like α-H [14].

We will assume that the bandage is being placed over a recent wound prior to the bacteria reaching stationary phase. As such, no α-H has yet been produced. We will begin modeling at the moment the wound reaches stationary phase and begins to produce α-H.

3.6.1 Wound:

In the wound, the initial concentration of α-H is zero. This is because the bacteria do not produce α-H until they reach stationary phase, and we are focusing on the moment the wound reaches stationary phase and onward. The concentration of dye in the wound is also zero initially. This is because the dye is stored in the vesicles in the wells. Without the presence of α-H, the vesicles will remain whole and cannot release the dye.

3.6.2 Hydrogel Main Body:

In the body of the wells, the initial concentration of α-H is zero. Again, this is because we are assuming that there has been no production of α-H before the moment we begin the model. The concentration of dye in the hydrogel main body is also zero, since no α-H is present to lyse the vesicles.

3.6.3 Hydrogel Wells:

In the wells, the initial concentration of α-H is zero as there has been no production of α-H. The concentration of dye in the wells is also zero initially. This is because the dye we are looking at is specifically free dye. Although there is technically dye present in the well, it is contained within the vesicles. Since the dye is not free (it has not been released from the vesicle through an α-H pore) it is not the species we are interested in.

4. Results and Discussion

4.1 Mesh Implementation:

4.1.1 Mesh Convergence:

Due to the nature of our model, two separate mesh convergence analyses were conducted, one for the wound domain and the other for the hydrogel domains (hydrogel main body and hydrogel wells). This was done because the domain of the wound is very thin compared to the domains of the hydrogel. Thus, the mesh of the wound would be very different from the mesh of the hydrogel.

The mesh settings we used were obtained from the COMSOL predetermined coarse, normal, fine, and finer settings when it was calibrated for fluid dynamics. The values for these parameters are shown in a table below:

Table 1: Values for mesh convergence settings

	Coarse	**Normal**	**Fine**	**Finer**
Maximum element size	1.1	0.737	0.583	0.407
Minimum element size	0.33	0.22	0.11	0.044
Maximum element growth rate	1.2	1.15	1.13	1.1
Curvature factor	0.7	0.6	0.5	0.4
Resolution of narrow regions	0.6	0.7	0.8	0.9

To conduct the mesh convergence on the wound, a point was selected at (1cm, 1cm, -10μm) to analyze how well the normal, fine and finer meshes converge for α-H diffusion since α-H is the most common species in the wound. The convergence analysis (Figure 6)

demonstrates that the fine mesh is the most efficient and accurate mesh for the domain of the wound.

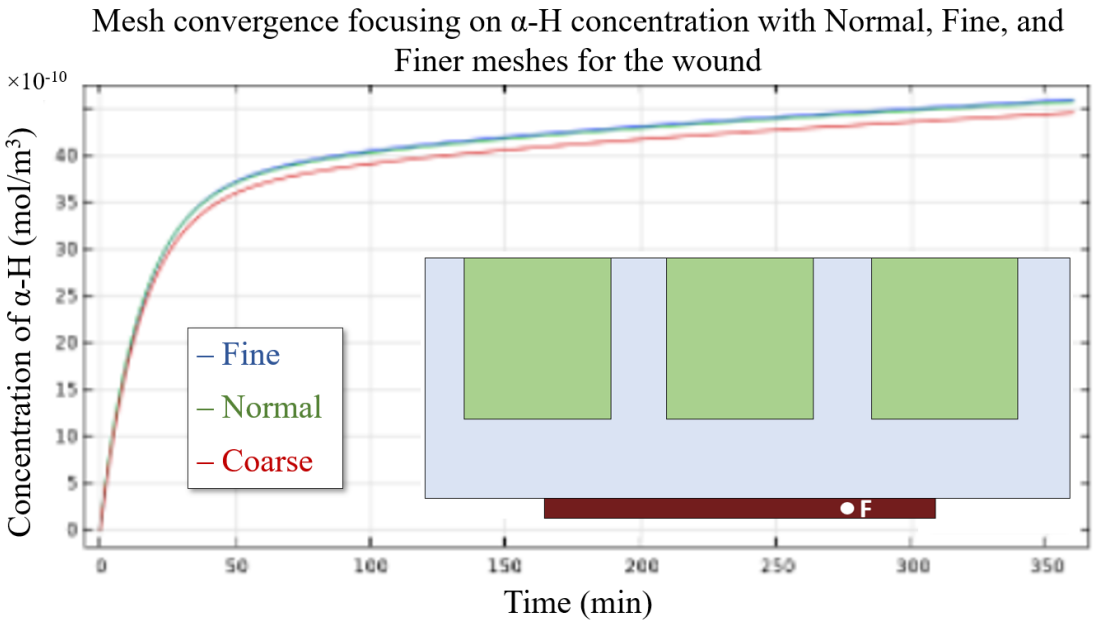

Figure 6: Convergence analysis for a 3D cut point at point F (1cm, 1cm, -10μm) in the domain of the wound for normal, fine, and finer meshes.

As shown in Figure 6, the Fine and Finer meshes are essentially indistinguishable. As such, we concluded that a Fine mesh was sufficient to model the domain of the wound.

To conduct the mesh convergence on the hydrogel main body, a point was selected to compare the coarse, normal, fine and finer meshes convergence for α-H diffusion, since α-H is the most common species in the hydrogel. This point is shown in Figure 12 as Point E. Because of insufficient memory, two separate mesh convergence analyses had to be performed with the first analysis running the fine, normal and coarse meshes and the second analysis running the fine and finer meshes, shown in Figure 7. The mesh convergence analyses demonstrate that the fine mesh is the most efficient and accurate mesh for the hydrogel domains.

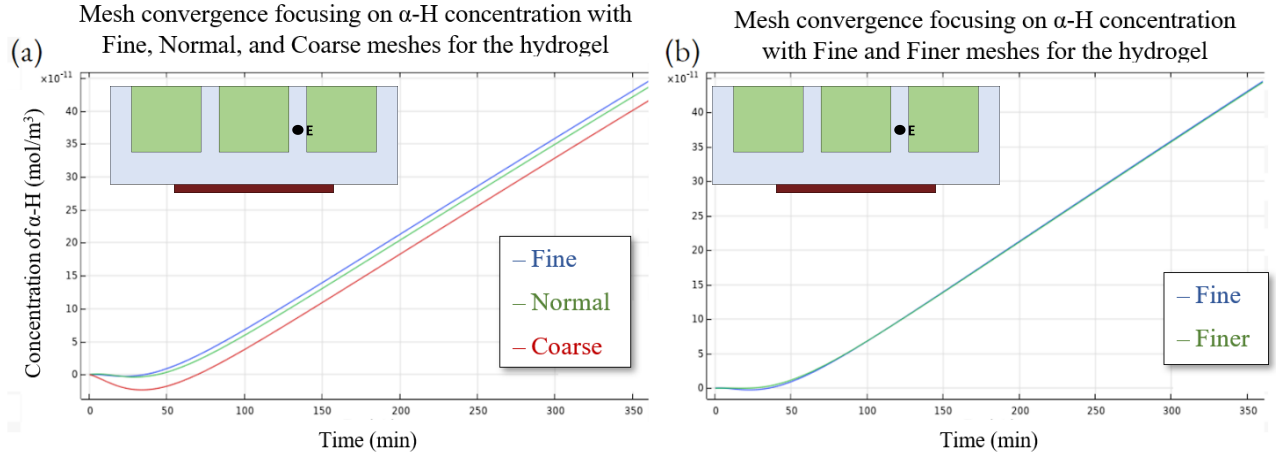

Figure 7: Mesh convergence analysis for a 3D cut point at (1cm, 1cm, 1mm) in the hydrogel domains. The cut point is shown in the overlay on the graph (a) Convergence analysis for fine, normal and coarse meshes. (b) Convergence analysis for fine and finer meshes.

4.1.2 Final Mesh:

From the mesh convergence, we determined that the optimal mesh for both the hydrogel domains and the wound domain was the COMSOL predefined fine mesh, shown below in Figure 8.

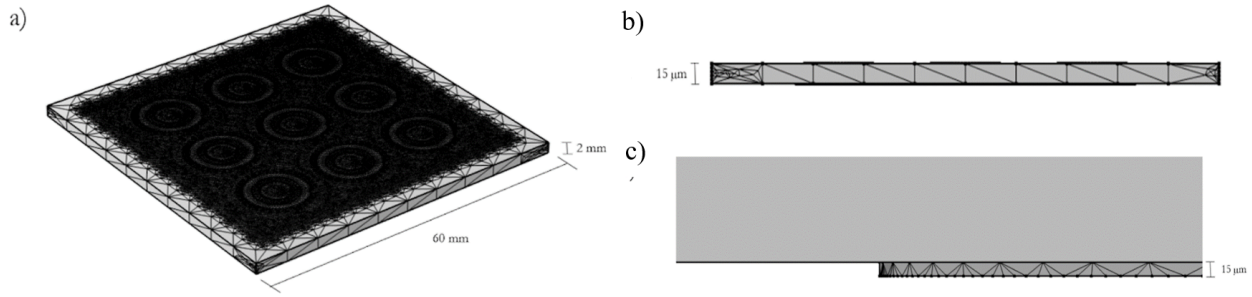

Figure 8: a) The mesh for the hydrogel bandage that was determined to be the best mesh by the mesh convergence in Figures 6 & 7. b) A side view of the wound's mesh c) An alternate side view of the wound's mesh.

4.2 Solution:

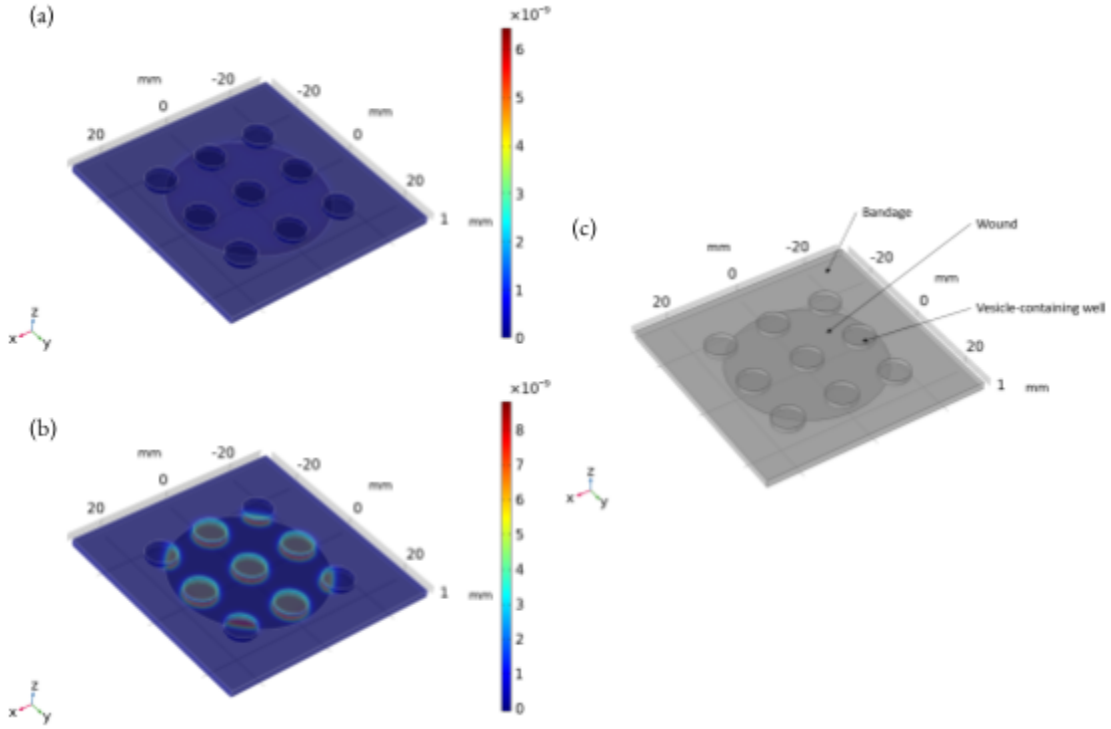

Figure 9: Final 3D concentration profile solution at t = 360 min for (a) α-H and (b) fluorescent dye. (c) shows the implemented geometry

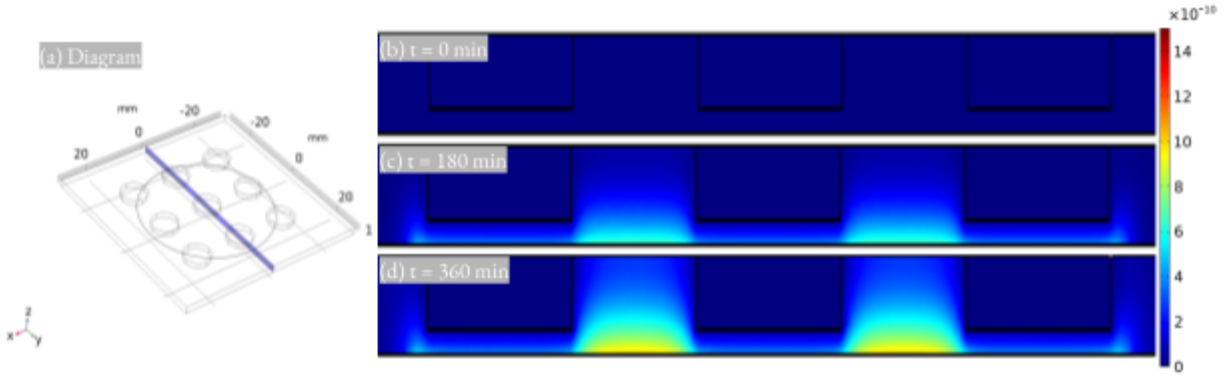

Figure 10: 2D concentration profile of α-H taken at a slice shown in (a) at 0 min shown in (b), 180 min shown in (c), and 360 min shown in (d).

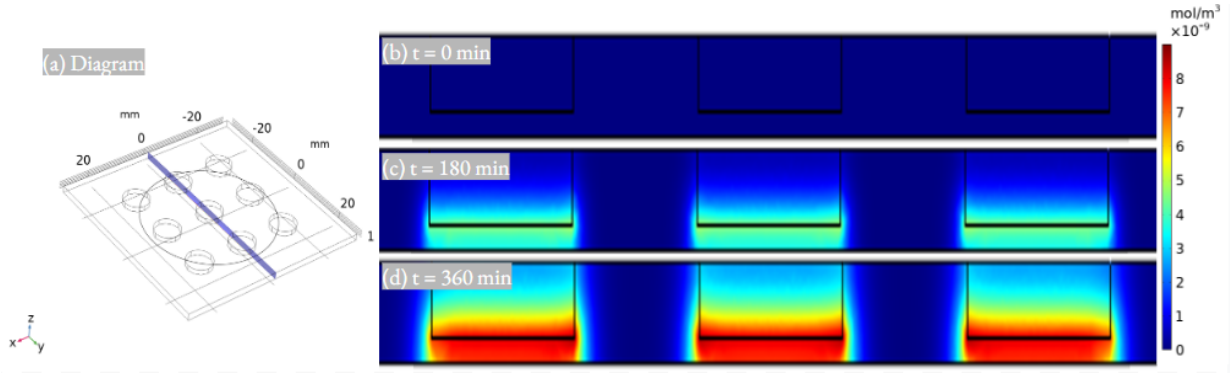

Figure 11: 2D concentration profile of fluorescent dye taken at a slice shown in (a) at 0 min shown in (b), 180 min shown in (c), and 360 min shown in (d).

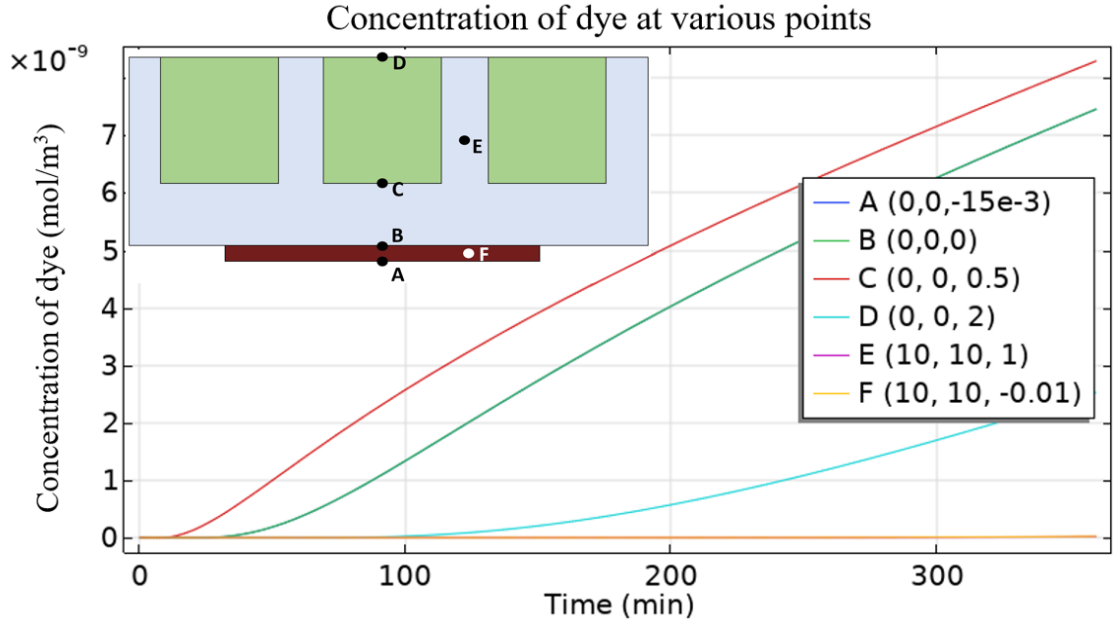

Figure 12: Concentration profiles of fluorescent dye in the bandage and wound over time at 6 points on the geometry. Initially there is no free dye present, as all of the dye is self-quenched inside of the vesicles. Once the α-H has diffused up through the bandage, it reaches the wells and lyses the vesicles. This releases the dye, and as the dye diffuses out it lowers in concentration and does not self-quench. The visible dye indicates that the wound is infected.

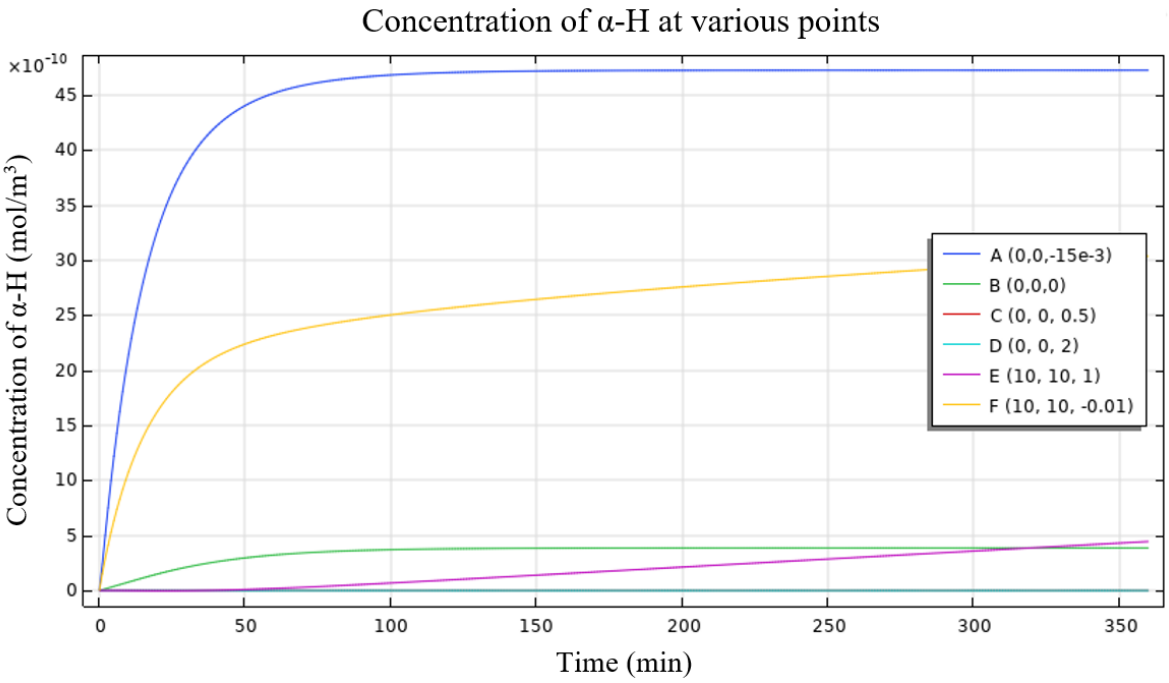

Figure 13: Concentration profiles of α-H in the bandage and wound over time at the same 6 points on the geometry as shown in Figure 12. Initially, large amounts of α-H are produced in the wound, causing it to diffuse into the hydrogel bandage. Once it reaches the well, the α-H is immediately used to create pores in the vesicles, causing the α-H concentration in the wells to be 0. This maintains the concentration gradient of α-H, causing the solution to eventually reach steady state.

As shown in Figure 10, initially there is no α-H present because t = 0 is when the bacterial colony first reaches stationary phase (when bacteria focus less on cell division and more on cytotoxin production). Over time, α-H diffuses through the wound and hydrogel main body into the wells where it reacts immediately with vesicles to form pores that release the dye. Thus, in Figure 10, there is no α-H present within the wells. Also, the α-H is used up when it reaches the wells. As such, there is essentially no buildup of α-H under the wells, unlike between them. As shown in Figure 11, there is no dye at t = 0 because no α-H has diffused into the wells yet so no dye has been released. However, over time, the α-H reaches the wells and causes dye to be released from the vesicles. The highest dye concentration would be at the area of contact between the hydrogel and the wells, as the infinite vesicle assumption means that dye will only be produced at that interface. The dye mainly diffuses up and down the bandage with minimal lateral diffusion from that spot over time, and would start glowing over the shown time-steps.

Our design goal is to minimize the amount of fluorescent dye that reaches the wound so as to avoid contamination, while still ensuring that the α-H reaches the wells in a reasonable amount of time. This balance will allow for rapid detection of infection, while leaving the wound clean and uncontaminated by dye.

4.3 Validation

To determine whether or not our model is reasonable, we must compare it with data others have obtained from real-life testing of related situations. The most clearly applicable experiment is the paper from which we drew our bandage design [15]. This paper found that the fluorescent dye was clearly visible to the naked eye after approximately 4 hours in contact with the "infected wound". Since we are modeling from the point when the wound becomes infected and onward, we expect our bandage to exhibit a clear, visible glow as well after the same time period of 4 hours after the wound has been infected.

To determine when the bandage begins to glow, we can analyze the light emitting properties of the dye in the wells. Although very little data was available for the dye in our model, 6-carboxyfluorescein, we were able to find information about a similar fluorescent dye: fluorescein (the only difference is an extra carboxyl group at the 6' carbon). It was found that the human eye is able to detect a minimum light intensity of 10^{-10} W/m^2 [16]. Given that each molecule of fluorescein can emit 30,000 photons and the dye emits light at a wavelength of 517 nm, we can determine the dye concentration required for the eye to be able to detect light [17, 18].

To do this, we can use the following equation to find light intensity, I, where n is the number of photons, f is the light frequency, h is Plank's constant, A is the incident area, and Δt is the unit time.

$$I = \frac{nfh}{A\Delta t} \tag{7}$$

We can acquire Equation 7 for light intensity from the commonly known equations below:

$$I = \frac{P}{A},\ P = \frac{E}{\Delta t} \tag{9}$$

$$\text{thus } I = \frac{E}{\Delta t \cdot A} \tag{10}$$

where P is power and E is energy. Because we care about intensity for a specified number of photons, n, we thus obtain the following equations for n photons specifically:

$$E = n \cdot hf = n \cdot hc/\lambda \tag{11}$$

where h is Planck's constant, λ is the wavelength of light emitted and c is the speed of light (3 x 10^8m/s). Substituting Equation 11 into E, we thus obtain Equation 7:

$$I = \frac{nch}{A\lambda\Delta t} = \frac{nfh}{A\Delta t} \tag{12}$$

Using this equation, we will calculate the number of excited 6-carboxyfluorescein molecules required to be visible to the naked eye. We know that the minimum intensity required for visibility by the naked eye is 10^{-10} W/m^2 [16]. Because a fluorescein dye molecule (which is extremely close to 6-carboxyfluorescein) emits 30,000 photons per fluorescein molecule, we can thus solve Equation 7 for the number of molecules (N) required for visible detection by the naked eye [18]:

$$10^{-10}\ \frac{W}{m^2} = \frac{30000\ photons/molecule \cdot N \cdot 3 \cdot 10^8 m/s \cdot 6.634\times10^{-34} J\cdot s}{517 \cdot 10^{-9} m \cdot 1s \cdot (\ 37.5^2 \cdot 0.004^2 \cdot 3.14\ )} \tag{13}$$

This equation shows that 612 molecules of free dye are required for the eye to detect light from our bandage. Avogadro's number converts this to $1.02 \cdot 10^{-21}$ moles of dye. Assuming these molecules are localized in the well, we find that a minimum dye concentration of $1.4 \cdot 10^{-14}$ mol/m^3 is required for the dye to be visible to the naked eye, so clear detection should be several orders of magnitude above this level. As shown in Figure 12, after four hours our bandage had a maximum dye concentration on the order of 10^{-9} mol/m^3. This is a clearly visible signal, since it is several times stronger than the minimum detectable signal. This result is validated by the results from the original SmartWound PREDICT bandage that showed a clear, visible response after four hours [15].

We can also compare the concentration of dye at 4 hours calculated in our model to that which was found in the original paper describing the SmartWound PREDICT bandage [15]. When they tested the SmartWound PREDICT bandage, they placed the bandage over a large biofilm and observed the fluorescence [15]. After 4 hours, one of the bandages had a fluorescence level of around 12,000 RFU (when normalized to the control), which correlates to a dye concentration of roughly $3 \cdot 10^{-6}$ M [19].

To adjust our model to the testing conditions for the SmartWound PREDICT bandage, we enlarged the radius of our wound so that it covered the entire bandage and increased the thickness and concentration of the bacteria to match biofilm conditions. We did this since the SmartWound PREDICT bandage was tested over a bacterial biofilm, not a typical wound. To implement this, we replaced the wound with a biofilm that was modeled as a cylinder with a radius of 60 mm and a thickness of 1002 μm to better resemble a large biofilm [33]. We also increased the concentration of bacteria to $5 \cdot 10^9 \frac{bacteria}{cm^3}$ to match the bacterial concentration of biofilms [34]. Substituting the new concentration of bacteria in the biofilm for the concentration of bacteria in the wound in Equation 3 provides us with the rate of α-H production in the biofilm given by the following calculation:

$$R_{\alpha-H,V,\ biofilm} = 9.6 \cdot 10^{-10} \frac{ng\ \alpha-H}{bacteria \cdot s} \cdot 5 \cdot 10^9\ \frac{bacteria}{cm^3} \cdot \frac{1}{5.4 \cdot 10^{-11}} \frac{molecules\ \alpha-H}{ng\ \alpha-H} = 8.9 \cdot 10^{10} \frac{molecules\ \alpha-H}{cm^3 \cdot s} \quad (14)$$

With these adjustments, our model found that the concentration of dye at the wells is $6.6 \cdot 10^{-6}$ M, giving us a 54.5% error. This is a reasonably close value because even miniscule errors or changes can be more impactful when the starting concentration is so minute. Also, since in reality the bacteria concentration increases and decreases as nutrients are used up, and the percent error is within one order of magnitude, we can say that the error is not significant.

Considering that these two methods for validation are based on experimental data, we are confident that our model accurately describes the physics of the actual SmartWound bandage.

4.4 Sensitivity Analysis

Because of the lack of documentation regarding the diffusivity of α-H and 6-carboxyfluorescein through a 2% agarose gel, we were only able to use the diffusivities of similarly sized molecules. As such, it is important to know how variation in the diffusivities will affect the final model. To determine how changes in diffusivity would affect the model, we

performed a sensitivity analysis on the diffusivity values of α-H and fluorescent dye, in which we varied each value by ±10% and observed the change in concentration at different points within our geometry. For α-H, we examine the concentration at Point E. For fluorescent dye, we examined the concentration at Point C since the dye is released near the bottom of the well where the vesicles first make contact with the α-H.

a)

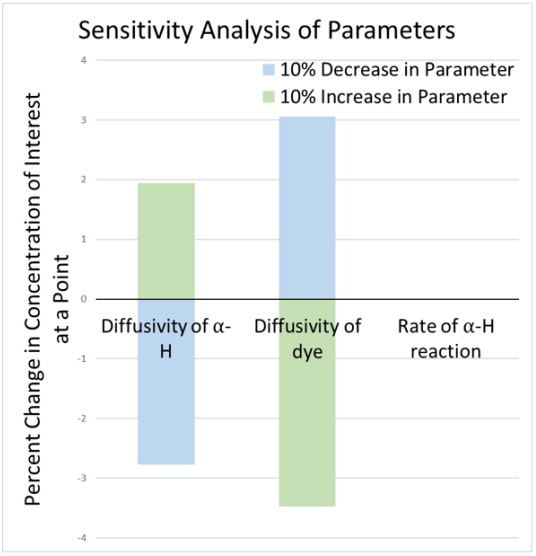

b)

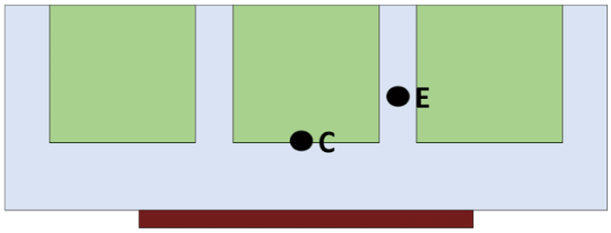

Figure 14: a) A bar plot showing the percent change in either the concentration of dye or α-H as the corresponding parameters are changed. The bars for changing the rate of α-H production are there, but are almost negligible (as shown in Figure 15) b) A visual representation of where we measured the change in α-H or dye.

As you can see in Figure 14, the concentration of α-H at point E is only minorly affected by changes in its diffusivity. After four hours, the concentration is only changed by approximately 3% in either direction. This difference appears fairly stable, and since we are only looking at the first few hours, it is unnecessary to look at how the concentration would be affected over many days. The differences also follow the expected pattern, with higher diffusivities allowing more α-H to reach point E from the wound more quickly. As such, it seems reasonable to conclude that small errors in the diffusivity of α-H will not have an excessive impact on the model. It is also important to understand how the concentration of dye throughout the bandage will be affected by changes in diffusivity.

We can also see that the diffusivity of the dye does have a visible impact on the concentration of dye at point C. Since the dye is diffusing away from point C, it is expected that the highest diffusivity would correspond to the lowest concentration, and vice versa. Figure 15 follows the expected trend, with a 10% increase and decrease in diffusivity leading to an approximately 3% decrease and increase in concentration respectively after four hours. This is not a large margin of error, so it seems unlikely that small errors in the diffusivity of dye would have undue impacts on the model. Although the error does seem to steadily increase over time, this should not be a problem in our model since we are only looking at the first few hours.

Another parameter that could impact the model is the rate of α-H uptake by the vesicles, which is described by the constant k_{eff}. This could impact both the rate of α-H degradation and the rate of fluorescent dye production, so it is important to understand the effect that alterations could have on the model. Since the dye production is proportional to the α-H degradation, it is only necessary to investigate the effect of changing k_{eff} on one of these values. We chose to investigate the α-H concentration at different values for k_{eff}.

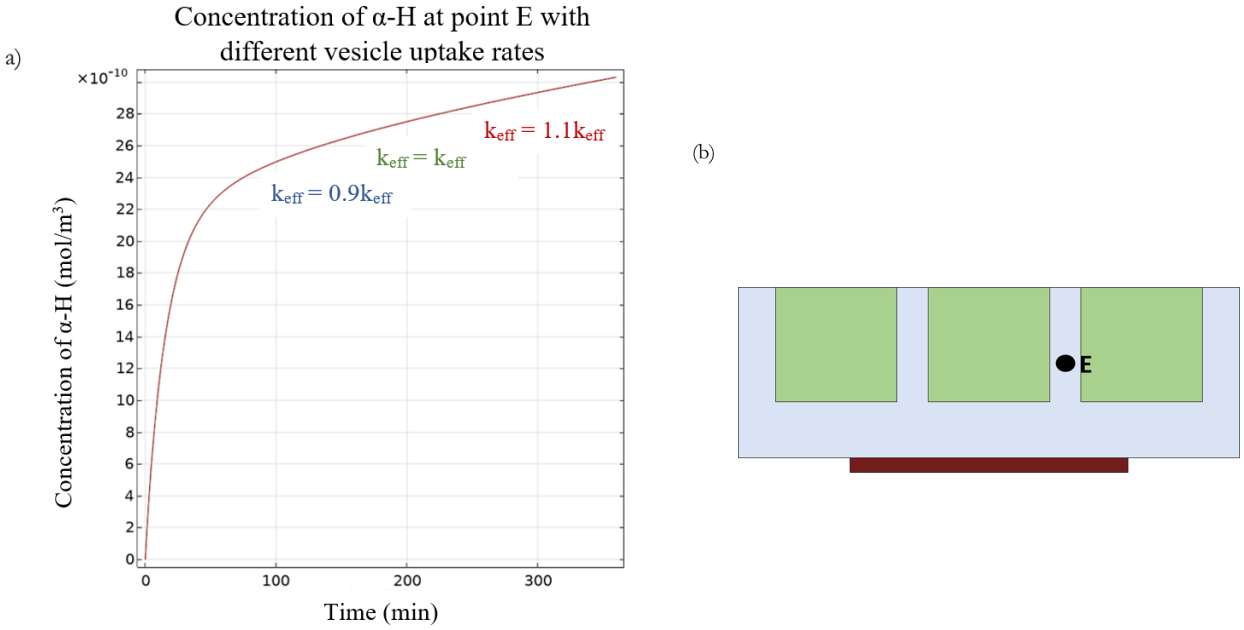

Figure 15: a) Concentration profile of α-H at point E over time at three different values for k_{eff}. The blue line is -10% to k_{eff} and the red line is +10% to k_{eff}. The change is almost negligible and the three lines are essentially overlaid on each other. Figure 15b shows the point at which the α-H concentration was measured.

Figure 15 shows that differences to our k_{eff} cause negligible differences in the concentration of α-H at point E. As such, it is likely that our rate of α-H degradation (which is dependent on this input constant) is fairly sound, and small changes will not have a large impact on the overall model. The fact that changing the k_{eff} does not change the concentration of α-H at Point E suggests that the assumption that we have an infinite reservoir of lipid vesicles is reasonable. If this were not a sound assumption, then changing the k_{eff} would have an effect on the concentration of α-H as diffusion of α-H into the bandage would be limited by the reaction between α-H and lipid vesicles. However, because this doesn't occur, it means that the production of dye is limited by the diffusion of α-H into bandage and not the reaction of α-H with the lipid vesicles.

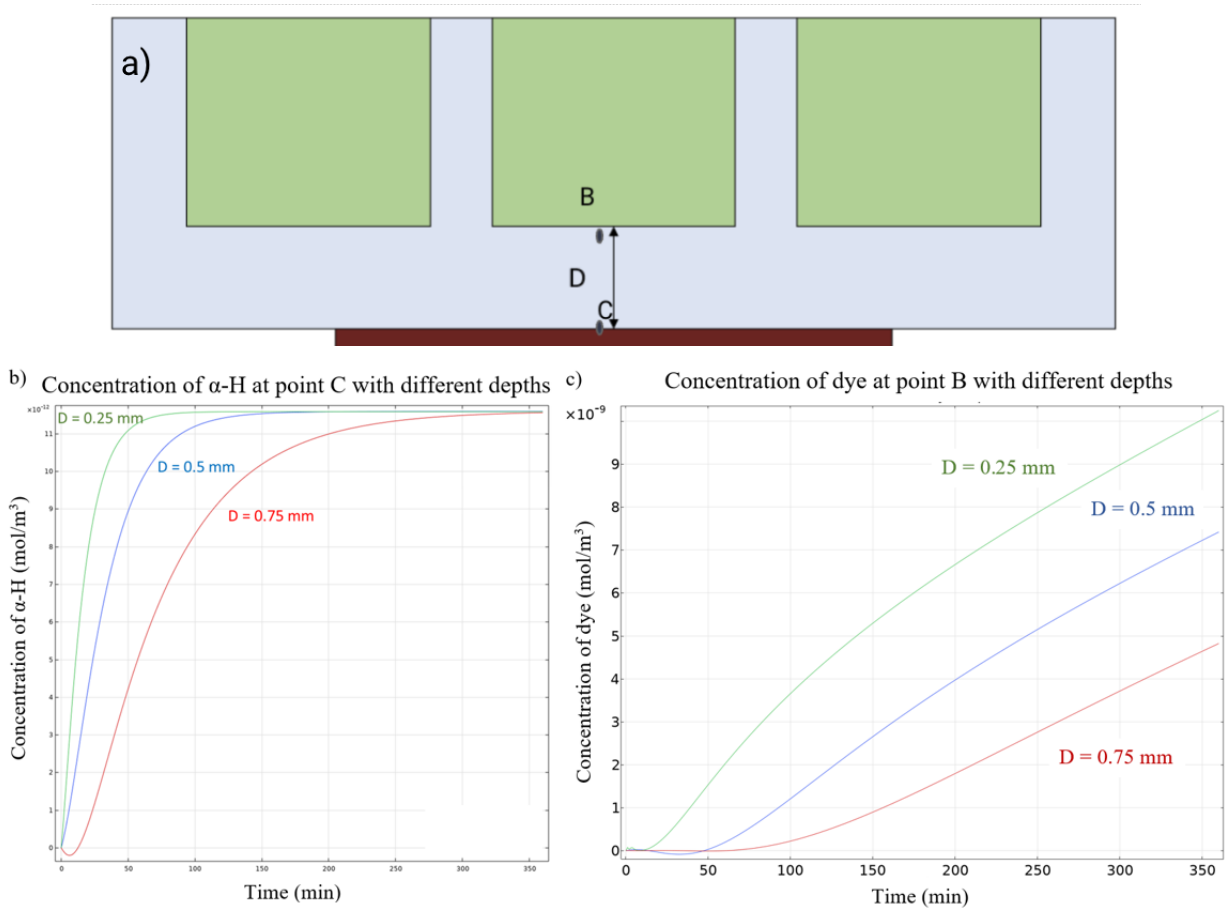

Figure 16. Concentration of α-H at point C and of dye at point B over time at different bandage depths.

In order to investigate the effects of changing bandage dimensions, we changed the depth of the hydrogel bandage (D value shown in Figure 16a). Our original design has D = 0.5 mm and we tested the smaller D value, 0.25 mm and larger D value, 0.75 mm. As shown in Figure 16 b&c, larger bandage depths lead to a longer diffusion time for both α-H and dye. Optimization of depth would require further research and optimization taking into account mechanical changes that come with decreasing bandage thickness.

5.1 Conclusion

We built a 3D COMSOL model of a smart hydrogel bandage that can detect the presence of bacterial pathogens such as *Staphylococcus aureus.* Once a wound becomes infected there are two possibilities: the body's immune system can defeat the invading pathogens, or they can multiply until reaching the stationary phase where they require treatment by antibiotics. When antibiotics are given too early, it leads to overuse that increases bacteria resistance. When they are given too late, the infection can already have become septic. To avoid these situations, it is important to understand when a wound first becomes sufficiently infected to the point of requiring antibiotics.

To address this issue, this bandage provides a timely notification that a wound has become infected. Like the original product it is based on, it provides a visible glow after only four hours in contact with the infected wound. When it is first placed on the fully infected wound, cytotoxins begin to diffuse up from the wound into the bandage. When these toxins reach the vesicle containing wells, they lyse the wells and release fluorescent dye. This fluorescent dye tells the user that they need to seek medical attention.

The insight into the process of α-H diffusion and dye release allowed us to form several recommendations about potential improvements to our model. These recommendations include measures to both decrease the cost of the bandage and improve the function:

5.1.1 Optimization of Dye Type

Since the SmartWound PREDICT bandage in our model used carboxyfluorescein as their dye, we chose to model the bandage with this dye. It has several benefits: it is self quenching, which is a necessity for this design (it must not fluoresce until the α-H has released it from the vesicles), and it is non-toxic and FDA-approved at concentrations less than 30 mg/kg (so it is safe for use in a medical device) [25]. Despite being safe at low concentrations, carboxyfluorescein's safety data sheet (SDS) advises avoiding contact with your skin, and washing thoroughly with soap and water if it comes into contact with skin [26]. This is because some studies have shown negative side effects to fluorescein within the body [25]. As such, if possible, the dye should not come into contact with bare skin. Because of this, one of our design goals was to avoid letting the dye come into contact with the wound. We considered optimizing several factors of the bandage to achieve this goal, including the concentration of agarose in the hydrogel body and the thickness of the bottom layer of gel.

Another potential way to avoid negative side effects from dye would be to change the dye molecule used. If the molecule were larger, it would have a lower diffusivity and would thus take longer to reach the skin. One such dye molecule is Sulforhodamine B. Sulforhodamine B is a self-quenching fluorescent dye. It is approximately twice as large as carboxyfluorescein, so it should take significantly longer to diffuse down to the wound once it has been released from the vesicles. It is non-toxic as well, although its SDS also recommends washing the skin with soap and water on contact as well. One extremely large benefit of the Sulforhodamine B is that it can be stored at room temperature [27]. Carboxyfluorescein, on the other hand, is only stable in the long term if it is stored at 2-8 degrees Celsius [26]. This could make sales difficult, since it would not have a long shelf life in stores unless it was kept in a refrigerated section. Also, it would complicate accessibility in developing countries, since access to refrigeration units may be less common. Essentially, the sulforhodamine seems to be a superior dye in all aspects but price. One kilogram of carboxyfluorescein can be purchased in bulk for one dollar, however one kilogram of sulforhodamine B costs slightly more than $100,000 [28, 29]. Unfortunately, this price difference makes the sulforhodamine impractical for mass production of the bandage. There are other options for self-quenching dyes, like calcein, but they pose their own problems; calcein is combustible, so it is not ideal to use for a bandage [30]. Carboxyfluorescein seems to be one of the most practical dyes for use given safety considerations and price.

5.1.2 UV Light Source

Typically, fluorophores require a strong light source in order to fluoresce; the stronger the light source, the more fluorescence. A UV lamp should be a strong enough source to cause the dye to fluoresce as the SmartWound paper uses one to view its bandage [15]. If the user wanted to view their bandage at home, they would need a UV lamp. This could be made very clear on the packaging instructions and the user would have to acquire one themselves. Alternatively, fabricating a UV flashlight with UV LEDs would not be hard and we could sell one along with the bandage.

5.1.3 Optimization of Form

From the concentration profiles we obtain, we can see that in 2% agarose, the dye will mostly diffuse downwards instead of sideways within the bandage. Therefore, it is imperative to optimize the thickness of the hydrogel between the wells and the wound so that the bandage releases a visible amount of carboxyfluorescein dye before it diffuses down towards the wound. Decreasing the depth of the layer of agarose separating the wound from the wells would decrease the amount of time it takes for the α-H to reach the wells. Since the α-H would reach the wells sooner, the bandage would begin to glow more quickly. Decreasing the depth would also decrease the price of producing the bandage, since less material would be used overall. There could be complications from this, however, as decreasing the depth could have unintended side effects since decreasing the thickness of the layer would also decrease the time for the dye to diffuse down into the wound. This would mean that the dye would reach and contaminate the wound more quickly. It could also decrease the structural integrity of the hydrogel bandage and make it easier to break. As such, this may not be an optimal parameter to target when seeking to optimize bandage design.

Although not all of the precise values describing this situation could be found in the literature, our sensitivity analysis showed that minor variations in parameters would not have a significant impact on our model. Thus, if future manufacturers want to increase the percentage of agarose in the hydrogel to increase the structural integrity of the bandage or decrease the percentage of agarose in the hydrogel to lower the cost of the bandage, it should not noticeably affect the diffusivity of α-H or fluorescent dye in the bandage or the integrity of the model.

Similarly, small changes in the concentration of vesicles in the wells should not have a large impact on the rate of dye appearance. This is because the current vesicle concentration is large enough to be essentially infinite over the time range that is useful for detection. Decreasing the vesicle concentration to the point where it is not essentially infinite would complicate the model, but it could be a useful future step to optimize the price of the bandage.

5.1.4 Impact of Model

With our model, many different designs of the bandage can be tested in a timely manner, saving both time and resources. Even if we did not want to change the physical design and only wanted to change some physical properties, such as percent agarose, concentration of lipid vesicles within the wells, or the fluorescent dye used, building every single bandage would take a significant amount of time and resources compared to running it through the model. Not only

that, the testing of new designs would mean that new molds and fabrication methods would have to be developed. However, considering we can change parameters and dimensions in COMSOL, building all these molds and developing these fabrication methods may not be necessary since we can test many different designs without the expense of fabrication. Thus, being able to test many different bandage designs with different properties in COMSOL before expending resources to physically form and test them would be invaluable.

Physically testing the model would be difficult as well if we were to do it experimentally. The SmartWound paper [15] tests their bandage on a biofilm, not an actual wound. However, as shown in our validation section, the bandage would react very differently to a biofilm compared to a burn wound. On top of that, shaping a biofilm to fit different wound shapes and sizes would be a difficult task. Therefore, the only real way to test the hydrogel bandage on wounds would be in animal models or *ex vivo* human skin models [2]. Both of these methods would take a lot of time and money, especially if we wanted to test a lot of new bandage designs physically. Thus, our model could be used to test different bandage designs on different wound types, shapes, and sizes. After this model determines the best bandage designs, we could then move to animal models, thus reducing the time and cost of optimizing this bandage.

Since this bandage would have two main components (agarose and water) it would not pose significant ecological problems. Agarose (a seaweed derivative) is biodegradable and water is nontoxic. The SDS for the dye also shows no known environmental dangers [26]. As such, we do not foresee any difficulties involving disposal. Similarly, we do not foresee any particularly negative consequences to production. Since the main component of production would involve mixing the water and agarose and allowing the mixture to set, it shouldn't involve much use of fossil fuels or chemicals that would have a negative impact on the planet. Similarly, we foresee no ethical issues with producing this product. The seaweed required to make the agarose can be ethically sourced, and if the production facility were to use renewable energy sources, it could have a negligible carbon footprint. Although α-H is absorbed into the bandage, it should not be necessary to take extra precautions when disposing of the bandage because α-H does not interact with epidermal tissue, only endothelial tissue [13]. Thus, unless the bandage is ingested, it should not pose any significant health hazards.

With this model, we can more accurately understand the physics behind the SmartWound PREDICT bandage. Using this information, we can optimize the device design to more efficiently and cost-effectively notify users if their burn wound is sufficiently infected to require medical intervention.

Appendix A: Mathematical Statement of the Problem and Parameters

The geometry/schematic of the problem can be found in the Methods section of the report. The exact governing equations that we solved are found below. They are the transient mass transfer equations. The convection term is removed because we have no fluid flow in our model.

Transient transport of α-H: $$\frac{\partial c_{\alpha-H}}{\partial t} = D_{\alpha-H}(\nabla^2 \cdot c_{\alpha-H}) + R_{\alpha-H} \quad (13)$$

Transient transport of dye: $$\frac{\partial c_{dye}}{\partial t} = D_{dye}(\nabla^2 \cdot c_{dye}) + R_{dye} \quad (14)$$

In the wound domain, we include a reaction term for α-H because α-H is being generated by the bacteria. The dye does not react with anything within the wound.

$$R_{\alpha-H} = 2.6 \cdot 10^6 \quad (15)$$

$$R_{dye} = 0$$

In the hydrogel bandage (excluding the wells), there is no reaction term for either of the species.

$$R_{\alpha-H} = 0 \quad (16)$$

$$R_{dye} = 0 \quad (17)$$

In the hydrogel wells, there is a reaction term for both the α-H and the dye. The α-H forms a pore within each lipid vesicle, which is essentially a consumption reaction as the α-H does not dissociate from the lipid vesicle after. The dye is released from each lysed vesicle and thus, is dependent on the rate of α-H consumption. For every 7 α-H monomers that form a pore in a lipid vesicle, 80 molecules of dye are released. Therefore, the reaction terms are:

$$R_{\alpha-H,\,well} = -k_{eff} c_{\alpha-H} \quad (17)$$

$$R_{dye,\,well} = \frac{80}{7} k_{eff} c_{\alpha-H} \quad (18)$$

We used a zero-flux boundary condition all around the boundary:

$$-D_{\alpha-H}(\nabla \cdot c_{\alpha-H}) = 0 \quad (19)$$

$$-D_{dye}(\nabla \cdot c_{dye}) = 0 \quad (20)$$

No dye exists in our system initially as all of the dye is encapsulated within the lipid vesicles. Since *Staphylococcus aureus* do not make any cytotoxins until they have reached the stationary phase and we start our modeling at that point, our initial condition for α-H will also be zero. Therefore, our initial conditions are:

$$c_{\alpha-H} = 0 \quad (21)$$

$$c_{dye} = 0 \quad (22)$$

everywhere in our domain.

Table 2: Input parameters used in the model

Symbol	Description	Units	Value
Variables in GE			
$c_{\alpha-H}$	Concentration of α-H	$\frac{mol}{cm^3}$	Variable of Interest
$c_{\alpha-H,\,weight}$	Concentration of α-H by weight	$\frac{ng}{cm^3}$	Variable of Interest
$R_{\alpha-H,\,individual}$	Bacterial production of α-H	$\frac{monomers\ A}{(bacteria)(s)}$	18
$R_{\alpha-H,\,volumetric}$	Net production of α-H	$\frac{monomers\ A}{(cm^3)(s)}$	$2 \cdot 10^6$
$R_{\alpha-H,\,moles}$	Net production of α-H in moles	$\frac{moles\ A}{(cm^3)(s)}$	$3.3 \cdot 10^{-18}$
$R_{\alpha-H,\,vol,\,biofilm}$	Net production of α-H in Biofilm	$\frac{monomers\ A}{(cm^3)(s)}$	$8.89 \cdot 10^{10}$
$R_{\alpha-H,\,moles,\,biofilm}$	Net production of α-H in moles in Biofilm	$\frac{moles\ A}{(cm^3)(s)}$	$1.48 \cdot 10^{-13}$
Diffusivities			
$D_{\alpha-H,\,wound}$ [20]	Diffusivity of α-H through the wound	$\frac{cm^2}{s}$	10^{-10}
$D_{\alpha-H,\,gel}$ [21]	Diffusivity of α-H through the agarose hydrogel	$\frac{cm^2}{s}$	$6.4 \cdot 10^{-7}$
$D_{dye,\,gel}$	Diffusivity of fluorescent dye in gel	$\frac{cm^2}{s}$	$5 \cdot 10^{-7}$
$D_{dye,\,wound}$	Diffusivity of dye in wound	$\frac{cm^2}{s}$	$1.8 \cdot 10^{-8}$
Dimensions			
A_{wound}	Surface area of wound	cm^2	12.57
d_{wound}	Depth of wound	μm	15
$W_{bacteria,\,dry}$ [23]	Dry weight of bacteria	g	$0.15\ (W_{bacteria,\,wet})$

$W_{bacteria,\,wet}$ [24]	Wet weight of bacteria	g	10^{-12}
$W_{\alpha-H}$	Weight of α-H monomer	ng	$5.4 \cdot 10^{-11}$
$A_{vesicle}$	Surface area of a single vesicle	cm^2	$5.03 \cdot 10^{-9}$
R_H	Hydrodynamic radius of the dye 6-fluorescein	Å	5.02
Miscellaneous Values			
k_{on}	Adsorption constant of α-H into a lipid bilayer	$\frac{cm}{s}$	43
k_{eff}	Effective reaction rate constant	$\frac{1}{s}$	2160
$c_{bacteria,\,number}$	Concentration of bacteria in wound	$\frac{bacteria}{cm^3}$	110,900
$c_{bacteria,biofilm}$	Concentration of bacteria in biofilm	$\frac{bacteria}{cm^3}$	$5 \cdot 10^5$
$c_{bacteria,\,weight}$	Concentration of bacteria in wound	$\frac{bacteria}{gram\ tissue}$	100,000
$c_{vesicle,\,well}$	Concentration of vesicles in well	$\frac{vesicles}{cm^3}$	$2 \cdot 10^{10}$
ρ_{skin} [22]	Density of skin	$\frac{kg}{m^3}$	1109
N_{av}	Avogadro's number	$\frac{molecules}{mole}$	$6.02 \cdot 10^{23}$

This table contains all of the dimensions, physical and chemical properties, and rate constants that we used in our model.

Appendix B: Solution Strategy

For our model, the PARDISO solver was used to solve the equations. We used strict BDF time stepping with 1 min time steps because when we used free BDF time steps, we would get impossible concentrations at t = 0 s. The relative tolerance was 0.005 while the absolute tolerance factor was 0.1.

```
<---- Compile Equations: Time Dependent in Study 1/Solution 1 (sol1) --------
Started at Apr 29, 2022 4:31:34 PM.
Geometry shape function: Linear Lagrange
Running on Intel64 Family 6 Model 151 Stepping 2, GenuineIntel.
Using 1 socket with 20 cores in total on JimyDellDT.
Available memory: 16.07 GB.
Time: 5 s.
Physical memory: 1.88 GB
Virtual memory: 2.05 GB
Ended at Apr 29, 2022 4:31:39 PM.
----- Compile Equations: Time Dependent in Study 1/Solution 1 (sol1) --------
```

```
COMSOL Multiphysics 5.6.0.401
[Apr 29, 2022 4:29 PM] Opened file: D:\COMSOL models\5530 COMSOL\Deadline 4 Model 3.25 1905.mph
[Apr 29, 2022 4:31 PM] Number of degrees of freedom solved for: 453702 (plus 2002490 internal DOFs).
[Apr 29, 2022 5:19 PM] Solution time (Study 1): 2878 s. (47 minutes, 58 seconds)
```

Figure A1: The CPU time taken, memory used and degrees of freedom solved.

Appendix C: Extra Visuals

Not applicable.

Appendix D: References

[1] D. J. Crowley, N. K. Kanakaris, and P. V. Giannoudis, "Debridement and wound closure of open fractures: The impact of the time factor on infection rates," *Injury*, vol. 38, no. 8, pp. 879–889, Aug. 2007, doi: 10.1016/j.injury.2007.01.012.

[2] C. Schaudinn *et al.*, "Development, standardization and testing of a bacterial wound infection model based on ex vivo human skin," *PLoS ONE*, vol. 12, no. 11, p. e0186946, Nov. 2017, doi: 10.1371/journal.pone.0186946.

[3] "SmartWound® PREDICT diagnostic dressing," *SmartWound*. https://www.smartwound.co.uk/smartwound-predict/ (accessed Feb. 18, 2022).

[4] R. Ikram, "Microbiological assessment of infected wounds - Best Tests Issue 19," *bpac*, Jun. 15, 2013. https://bpac.org.nz/BT/2013/June/infected-wounds.aspx (accessed Apr. 21, 2022).

[5] A. Badarau, N. Trstenjak, and E. Nagy, "Structure and Function of the Two-Component Cytotoxins of Staphylococcus aureus – Learnings for Designing Novel Therapeutics," in *Protein Reviews*, vol. 966, M. Z. Atassi, Ed. Singapore: Springer Singapore, 2017, pp. 15–35. doi: 10.1007/5584_2016_200.

[6] J. S. Choi and K. Y. Kim, "Factors associated with preventive behaviors in the overuse and misuse of antibiotics in Korean nursing students," *American Journal of Infection Control*, vol. 47, no. 6, pp. 715–717, Jun. 2019, doi: 10.1016/j.ajic.2018.11.006.

[7] T. Sugawara *et al.*, "Structural basis for pore-forming mechanism of staphylococcal α-hemolysin," *Toxicon*, vol. 108, pp. 226–231, Dec. 2015, doi: 10.1016/j.toxicon.2015.09.033.

[8] R. F. Chen and J. R. Knutson, "Mechanism of fluorescence concentration quenching of carboxyfluorescein in liposomes: Energy transfer to nonfluorescent dimers," *Analytical Biochemistry*, vol. 172, no. 1, pp. 61–77, Jul. 1988, doi: 10.1016/0003-2697(88)90412-5.

[9] K. B. Johnsen, J. M. Gudbergsson, T. L. Andresen, and J. B. Simonsen, "What is the blood concentration of extracellular vesicles? Implications for the use of extracellular vesicles as blood-borne biomarkers of cancer," *Biochimica et Biophysica Acta (BBA) - Reviews on Cancer*, vol. 1871, no. 1, pp. 109–116, Jan. 2019, doi: 10.1016/j.bbcan.2018.11.006.

[10] R. Watanabe *et al.*, "Arrayed lipid bilayer chambers allow single-molecule analysis of membrane transporter activity," *Nat Commun*, vol. 5, no. 1, p. 4519, Dec. 2014, doi: 10.1038/ncomms5519.

[11] T. Larkin, "2020: Curious Kids: why don't burns bleed? - University of Wollongong – UOW," Feb. 19, 2020. https://www.uow.edu.au/media/2020/curious-kids-why-dont-burns-bleed.php (accessed Mar. 21, 2022).

[12] J. Chalmeau, N. Monina, J. Shin, C. Vieu, V. Noireaux, "α-Hemolysin pore formation into a supported phospholipid bilayer using cell-free expression," *Biochimica et Biophysica Acta (BBA) - Biomembranes*, vol. 1808, no. 1, pp. 271-278, 2011, https://doi.org/10.1016/j.bbamem.2010.07.027.

[13] S. L. Kaplan, K. G. Hulten, and E. O. Mason, "STAPHYLOCOCCUS AUREUS INFECTIONS (COAGULASE-POSITIVE STAPHYLOCOCCI)," in *Feigin and Cherry's Textbook of Pediatric Infectious Diseases*, Elsevier, 2009, pp. 1197–1213. doi: 10.1016/B978-1-4160-4044-6.50096-0.

[14] J. Freer and J. Arbuthnoti, "Toxins of staphylococcus aureus," *Pharmacology & Therapeutics*, vol. 19, no. 1, pp. 55–106, 1982, doi: 10.1016/0163-7258(82)90042-0.

[15] N. T. Thet *et al.*, "Prototype Development of the Intelligent Hydrogel Wound Dressing and Its Efficacy in the Detection of Model Pathogenic Wound Biofilms," *ACS Appl. Mater. Interfaces*, vol. 8, no. 24, pp. 14909–14919, Jun. 2016, doi: 10.1021/acsami.5b07372.

[16] Sharma, B.M., *Objective Physics for JEE: Class XII*, 1st ed. Cengage Learning India Pvt. Ltd., 2019.

[17] National Center for Biotechnology Information, "PubChem Compound Summary for CID 76806, 6-Carboxyfluorescein." https://pubchem.ncbi.nlm.nih.gov/compound/76806 (accessed Apr. 21, 2022).

[18] Q. Zhao, I. T. Young, and J. G. S. de Jong, "Photon budget analysis for fluorescence lifetime imaging microscopy," *J. Biomed. Opt.*, vol. 16, no. 8, p. 086007, 2011, doi: 10.1117/1.3608997.

[19] S. Milo, F. B. Acosta, H. J. Hathaway, L. A. Wallace, N. T. Thet, and A. T. A. Jenkins, "Development of an Infection-Responsive Fluorescent Sensor for the Early Detection of Urinary Catheter Blockage," *ACS Sens.*, vol. 3, no. 3, pp. 612–617, Mar. 2018, doi: 10.1021/acssensors.7b00861.

[20] R. J. Scheuplein, "Permeability Of The Skin: A Review Of Major Concepts And Some New Developments," *Journal of Investigative Dermatology*, vol. 67, no. 5, Part 2, pp. 672–676, Nov. 1976, doi: 10.1111/1523-1747.ep12544513.

[21] A. Pluen, P. A. Netti, R. K. Jain, and D. A. Berk, "Diffusion of Macromolecules in Agarose Gels: Comparison of Linear and Globular Configurations," *Biophysical Journal*, vol. 77, no. 1, pp. 542–552, Jul. 1999, doi: 10.1016/S0006-3495(99)76911-0.

[22] B. Lloyd, "Density » IT'IS Foundation," *ITIS Foundation*, 2022.

[23] L. R. Bakken and R. A. Olsen, "Buoyant Densities and Dry-Matter Contents of Microorganisms: Conversion of a Measured Biovolume into Biomass," *Appl Environ Microbiol*, vol. 45, no. 4, pp. 1188–1195, Apr. 1983, doi: 10.1128/aem.45.4.1188-1195.1983.

[24] L. Siu, "Mass of a Bacterium - The Physics Factbook," *The Physics Factbook*, 2003. https://hypertextbook.com/facts/2003/LouisSiu.shtml (accessed Feb. 25, 2022).

[25] R. Alford, H. M. Simpson, J. Duberman, G. C. Hill, M. Ogawa, C. Regino, H. Kobayashi, and P. L. Choyke, "Toxicity of organic fluorophores used in Molecular Imaging: Literature Review," *Molecular Imaging*, vol. 8, no. 6, pp. 1137–1150, Nov. 2009, https://doi.org/10.2310/7290.2009.00031

[26] "6-carboxyfluorescein Safety Data Sheet," *Sigma-Aldrich*. [Online]. Available: https://www.sigmaaldrich.com/US/en/product/sigma/c0662. [Accessed: 04-May-2022].

[27] "Sulforhodamine B Safety Data Sheet," *Sigma-Aldrich*. [Online]. Available: https://www.sigmaaldrich.com/US/en/sds/aldrich/230162. [Accessed: 04-May-2022].

[28] " 6-Carboxyfluorescein CAS 3301-79-9," *Alibaba*. [Online]. Available: https://www.alibaba.com/product-detail/Big-discounts-6-FAM-6-Carboxyfluorescein_1600502554153.html?spm=a2700.galleryofferlist.normal_offer.d_title.612b6b65cQLRZu. [Accessed: 03-May-2022].

[29] "Sulforhodamine B," *Sigma-Aldrich*. [Online]. Available: https://www.sigmaaldrich.com/US/en/product/aldrich/230162. [Accessed: 04-May-2022].

[30] "Calcein," *Thermo Fisher Scientific - US*. [Online]. Available: https://www.thermofisher.com/order/catalog/product/C1430. [Accessed: 04-May-2022].

[31] R. M. Donlan, "Biofilms: Microbial Life on Surfaces," *Emerg Infect Dis*, vol. 8, no. 9, pp. 881–890, Sep. 2002, doi: 10.3201/eid0809.020063.

[32] M. E. Olson, H. Ceri, D. W. Morck, A. G. Buret, and R. R. Read, "Biofilm bacteria: formation and comparative susceptibility to antibiotics," *Can J Vet Res*, vol. 66, no. 2, pp. 86–92, Apr. 2002.

[33] R. Bakke, P.Q. Olsson,Biofilm thickness measurements by light microscopy, Journal of Microbiological Methods, Volume 5, Issue 2, 1986, Pages 93-98, ISSN 0167-7012, https://doi.org/10.1016/0167-7012(86)90005-9.

[34] Sjollema, J., Rustema-Abbing, M., van der Mei, H. C., & Busscher, H. J. (2011). Generalized relationship between numbers of bacteria and their viability in biofilms. *Applied and environmental microbiology*, *77*(14), 5027–5029. https://doi.org/10.1128/AEM.00178-11